International Journal of Nanomedicine Dovepress

Open Access Full Text Article ORIGINAL RESEARCH

Targeted Liposomal Co-Delivery Dopamine with 3-n-Butylphthalide for Effective Against Parkinson's Disease in Mice Model

Yi Liang[1,2], Liping Feng[1], Yue Zheng[1], Yunzhen Gao[2], Rongying Shi[2], Zhirong Zhang[2], Xue Ying[1], Yingchun Zeng[1]

[1]School of Pharmacy, Chengdu Medical College, Chengdu, 610500, People's Republic of China; [2]Key Laboratory of Drug-Targeting and Drug Delivery System, Ministry of Education, West China School of Pharmacy, Sichuan University, Chengdu, 610041, People's Republic of China

Correspondence: Xue Ying; Yingchun Zeng, School of Pharmacy, Chengdu Medical College, No. 783, Xindu Avenue, Chengdu, 610500, People's Republic of China, Tel +86-28-62739552; +86-28-62739516, Email Yingxueshzu@163.com; zych19900119@163.com

Introduction: Parkinson's disease (PD) is a multifactor-induced neurodegenerative disease with high incidence in the elderly population. We found for the first time that the combination of dopamine (DA) and 3-n-butylphthalide (NBP) has great potential for the synergistic treatment of PD. To further improve the therapeutic performance of the drugs, a brain-targeting liposomal co-delivery system encapsulating NBP and DA ((NBP+DA)-Lips-RVG29) was designed using a rabies virus polypeptide with 29 amino acids (RVG29) as the targeting ligand.

Methods: The synergistic neuroprotective effects of NBP and DA were assessed in 6-OHDA-induced PC12 cells. Then, (NBP+DA)-Lips-RVG29 loading with NBP and DA at an optimal ratio was prepared using the thin-film hydration and sonication method. The physicochemical and biological characterization of (NBP+DA)-Lips-RVG29 were systemically investigated, and the therapeutic efficiency and underlying mechanisms of (NBP+DA)-Lips-RVG29 were also explored in vitro and in vivo. Finally, the safety of (NBP+DA)-Lips-RVG29 was evaluated.

Results: The synergistic effects of NBP and DA peaked at 1:1 (NBP/DA, mol/mol). The functionalized liposomes showed significantly higher uptake efficiency and blood-brain barrier (BBB) penetration efficiency in vitro. After systemic administration, (NBP+DA)-Lips-RVG29 prolonged the blood circulation of drugs, enhanced BBB penetration and increased drug accumulation in the striatum, substantia nigra and hippocampus. Moreover, (NBP+DA)-Lips-RVG29 showed excellent neuroprotective effects in a cellular PD model of PC12 cells and improved therapeutic efficacy in a PD mouse model. Furthermore, the safety evaluation of (NBP+DA)-Lips-RVG29 revealed no systemic toxicity.

Conclusion: NBP and DA exhibited the synergistic anti-PD effects. The RVG29-modified liposomes encapsulating NBP and DA contributed to the accumulation of drugs in the brain lesions area of PD and further improved treatment efficacy. Therefore, (NBP+DA)-Lips-RVG29 represents a promising strategy for the treatment of PD and other neurodegenerative diseases.

Keywords: Parkinson's disease, brain targeting, liposomes, dopamine, 3-n-butylphthalide, synergistic effect

Introduction

Parkinson's disease (PD), also known as paralysis agitans, is the second most common neurodegenerative disease after Alzheimer's disease. With the arrival of the aging population and the younger onset of PD, the incidence and mortality of PD are expected to increase markedly over the coming decades.[1] It is estimated that by 2030, the population of PD patients in China will account for more than 50% of the global patients.[2] The main pathological manifestations of PD are the loss of dopaminergic substantia nigra neurons and the formation of Lewy bodies mainly consisting of misfolded α-synuclein (α-Syn).[3] Currently, the available treatments for PD merely improve clinical symptoms but cannot slow or prevent disease progression.[4] Thus, there is an urgent need to develop new strategies to improve the effectiveness of PD treatments.

Received: 24 June 2024
Accepted: 14 November 2024
Published: 30 November 2024

Graphical Abstract

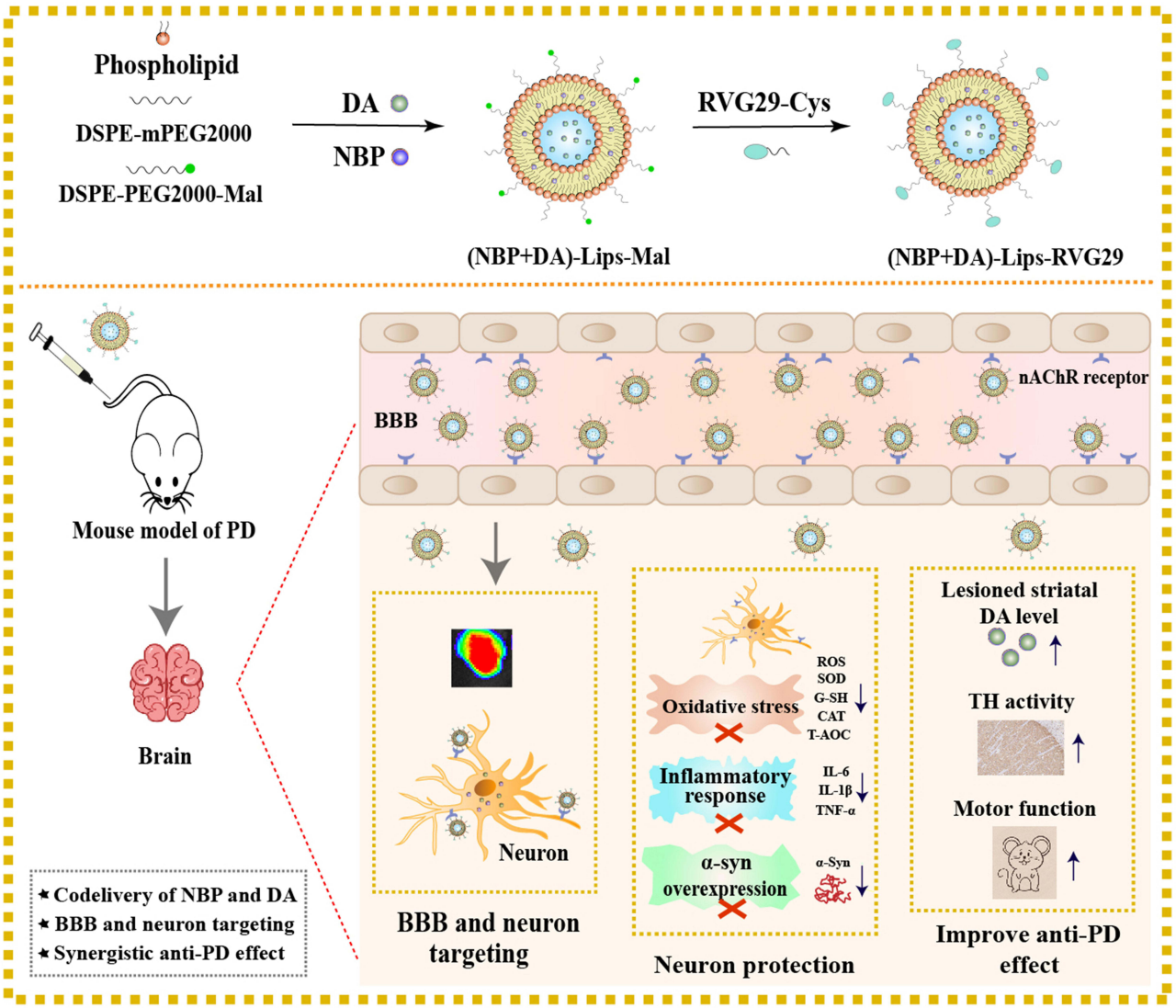

However, the pathogenesis of PD remains unclear. Numerous studies have shown that many pathogenic factors are associated with the development of PD, including oxidative stress,[5] mitochondrial dysfunction,[6] toxic protein aggregation[7] and inflammatory response.[8] Due to the complex mechanisms of PD, medication for any single factor may not achieve the ideal therapeutic effect. Therefore, drug combination strategies show bright prospect in PD therapy.

Current drug treatments for PD primarily focus on dopamine (DA) replacement strategy using levodopa (L-DOPA, a precursor of DA). L-DOPA is the "gold-standard drug available for the treatment of PD. However, only 1% given L-DOPA could cross the blood-brain barrier (BBB), and then be metabolized into DA to supplement the lack of DA in the brain.[9] To date, DA supplementation is the most direct and effective way to relieve the clinical symptoms of PD, but it could not improve the continuous occurrence of neurodegenerative lesions.[10,11] 3-n-butylphthalide (NBP), isolated from Apium graveolens seeds, is mainly used in the treatment of ischemic stroke.[12] It has many pharmacological activities, such as inhibiting neuroinflammation and apoptosis, promoting the degradation of α-Syn, reducing the generation and accumulation of reactive oxygen species (ROS) and repairing the neuronal damage.[13–16] More importantly, it has been shown to reduce the loss of DA neurons in preclinical PD models.[17] We speculated that NBP could

make up for the insufficiency of single DA therapy to a certain extent. In our study, we discovered that the combination of NBP and DA has great potential for the synergistic treatment of PD.

However, it's difficult for conventional drugs to pass through the BBB, and they have no site-specific distribution in the brain.[18] So, delivery of DA and NBP to the cerebral lesion site of PD with optimal proportional is key to achieving synergistic efficacy in vivo. Co-encapsulation of dual drugs using nanocarriers can optimize and unify the absorption and distribution behavior of different drugs in vivo.[19] Due to the potential toxicity issues, most nanomaterials are not suitable for brain-targeted drug delivery. Liposomes, mainly composed of non-toxic phospholipids and cholesterol, possess the properties such as bio-compatibility, bio-degradability and low toxicity, showing good prospects in clinical application prospects.[20] Moreover, liposomes have a "shell-core" structure, which can realize the simultaneous loading of hydrophilic drugs and lipophilic drugs. Therefore, liposomes are ideal nanocarriers for the brain-targeted delivery of NBP and DA.

In this study, we constructed a liposomal co-delivery system (NBP+DA)-Lips-RVG29 encapsulating NBP and DA for the treatment of PD. Liposomes were modified with the brain targeting peptide RVG29. RVG29 is a 29-amino acid peptide derived from rabies virus glycoprotein.[21] It can specifically bind to the highly-expressed acetylcholine receptor (nAChR) on brain capillary endothelial cells and brain neurons.[22] RVG29 is expected to facilitate drugs to efficiently penetrate the blood-brain barrier (BBB) and target to the diseased region of PD, resulting in the synergistic anti-PD effect of NBP and DA. In this study, the physicochemical and biological characterization of (NBP+DA)-Lips-RVG29 were systemically investigated, and the therapeutic efficiency and underlying mechanisms of (NBP+DA)-Lips-RVG29 were also explored in vitro and in vivo. Together, these findings may provide novel insights into the therapy of PD as well as other central nervous system diseases.

Materials and Methods

RVG29 peptide (YTIWMPENPRPGTPCDIFTNSRGKRASNG-Cysteine, RVG29-Cys) was synthesized according to standard solid-phase peptide synthesis by Shanghai Apeptide Co., Ltd. (Shanghai, China). DA (98% purity) was purchased from Solarbio Science&Technology Co., Ltd. (Beijing, China). NBP (99% purity) was purchased from Kemike Biomedical Technology Co., Ltd. (Wuhan, China). 6-hydroxydopamine (6-OHDA) was obtained from Aladdin Bio-Chem Technology Co., Ltd. (Shanghai, China). Soybean lecithin (S100) was obtained from Yuan Leaf Biotechnology Co., Ltd. (Shanghai, China). DSPE-PEG2000-Mal and DSPE-mPEG2000 were supplied by Ponsure Biotechnology Co., Ltd. (Shanghai, China). Cholesterol was purchased from Macklin Biochemical Co., Ltd. (Shanghai, China). 1,1′-dioctadecyl-3,3,3′,3′-tetramethylindodicarbocyanine, 4-chlorobenzenesulfonate salt (DiD) and 4,6-diamino-2-phenyl indole (DAPI) were obtained from Biotium (Hayward, California, USA). All other chemicals and reagents were obtained from commercial sources.

The Preclinical Trail Using Both Cell Lines and Animal Model

PC12 cells (rat adrenal pheochromocytoma cell line) were obtained from the Chinese Academy of Science Cell Bank (Shanghai, China) and cultured in RPMI-1640 medium (Kaiji Biotechnology Co., Ltd., Jiangsu, China). bEnd.3 cells (murine brain endothelial cell line) and JAWS II cells (murine dendritic cell line) were purchased from the American Tissue Culture Collection and cultured in Dulbecco's Modified Eagles Medium (DMEM, Kaiji Biotechnology Co., Ltd., Jiangsu, China). RPMI-1640 and DMEM were supplemented with 10% fetal bovine serum (FBS) and 5% streptomycin/penicillin.

Kunming mice (male, 40 ± 2 g) and Sprague-Dawley rats (male, 200 ± 10 g) were purchased from the Dossy Experimental Animal Co., Ltd. (Chengdu, China). All animal procedures were approved by the Institutional Animal Care and Ethics Committee of Sichuan University (Chengdu, China, KS2020022).

Synergistic Effects of 3-n-Butylphthalide and Dopamine in the 6-OHDA-Treated PC12 Cells

The synergistic effects of NBP and DA were evaluated in the 6-OHDA-treated PC12 cells.[23] PC12 cells were seeded in 96-well culture plates (2×10^4 cells/well) for the cell viability assay or in 12-well culture plates (1×10^5 cells/well) for

ROS and cell apoptosis assays. When cells nearly grew up to 80–90% confluence, the original cell culture medium was discarded, then serum- and antibiotics-free medium (control) and various combinations of free NBP and DA (NBP: DA = 1:8–8:1, mol/mol; final drug concentration, 100 μM) were added to each well and the cells were incubated for another 2 h. Next, 6-OHDA was added at a final concentration of 100 μM, and the cells were incubated for another 24 h.

Cell viability was measured using the 3-(4,5-dimethyl-2-thiazolyl)-2,5-diphenyl-2-H-tetrazolium bromide (MTT) method as described previously.[23] At the end of each treatment, the medium was replaced with 100 μL of MTT solution (1 mg/mL) and plates were incubated at 37 °C for another 4 h. Then, the insoluble formazan was dissolved in 150 μL of dimethyl sulfoxide (DMSO). The absorbance was measured at 490 nm using a microplate reader (Varioskan® Flash, Thermo Fisher Scientific, USA). The cell viability (%) was calculated according to the equation: $(A_{test}/A_{control}) \times 100\%$.

Intracellular ROS were quantified using a commercial kit (Beyotime, Jiangsu, China) with DCFH-DA as a fluorescent probe following the manufacturer's instructions.[24] Briefly, cells were loaded with 10 μM 2′,7′-Dichlorodihydrofluorescein diacetate (DCFH-DA) in all wells after treatment. After culturing for 20 min in the dark, the cells were analyzed using a Cytomics FC500 flow cytometer (Beckman Coulter, Miami, FL, USA).

The quantitative detection of apoptosis in PC12 cells from different groups was conducted by Annexin V-fluorescein isothiocyanate/propidium iodide (Annexin V-FITC/PI) Apoptosis Detection Kit (Bioscience, Shanghai, China).[25] After incubation, the cells were trypsinized, washed with ice-cold phosphate buffer solution (PBS), resuspended in binding buffer, and stained with Annexin V-FITC and PI. Then, the cells were incubated at room temperature in the dark and analyzed by flow cytometry after 15 min.

Preparation and Characterization of Liposomes

Liposomes were prepared by the thin-film hydration and sonication method.[26] The lipid compositions S100, DSPE-mPEG2000, DSPE-PEG2000-Mal and cholesterol (6:1:1:2, w/w/w/w) were dissolved in dichloromethane. The organic solvent was removed by rotary evaporation at 37 °C to form a uniform lipid film. The thin film was hydrated in 5% glucose solution and sonicated for 5 min at 100 W to obtain the maleimide-derivatized PEGylated liposomes (Lips-Mal). The PEGylated liposomes (Lips) were prepared using the same method with S100, DSPE-mPEG2000 and cholesterol (3:1:1, w/w/w). Then, RVG29-Cys (RVG29-Cys: maleimide group = 6:5, mol/mol) was added to the Lips-Mal solution. After stirring slowly at room temperature for 24 h, RVG29 peptide-modified liposomes (Lips-RVG29) were prepared via a maleimide and thiol coupling reaction. The successful conjugation of DSPE-PEG2000-Mal and RVG29 was confirmed by tricine-sodium dodecyl sulfate-polyacrylamide gel electrophoresis (Tricine-SDS-PAGE). The coupling rate of RVG29 was determined by the Ellman test (Solarbio). The amount of RVG29 on the liposomes was determined using a Micro BCA Protein Assay Kit (Thermo Fisher Scientific, Waltham, MA, USA), and the modification density of RVG29 on liposomes (proteins/lipids, mol/mol) was calculated.

NBP- and DA-loaded liposomes (NBP+DA)-Lips and (NBP+DA)-Lips-RVG29 were prepared by adding drugs (total drugs:lipids = 1:9, w/w) to the organic solution containing lipid components prior to the solvent evaporation. The liposomes and free drugs were separated by a Sephadex G-75 column (Yuanye, Shanghai, China). Similarly, NBP-Lips-RVG29, DA-Lips-RVG29, DiD-Lips and DiD-Lips-RVG29 were also successfully prepared.

The size, polydispersity index (PDI) and zeta potential of the liposomes were determined by Zetasizer Nano ZS90 dynamic light scattering (DLS, Malvern, UK). The morphology of Lips, Lips-RVG29 and (NBP+DA)-Lips-RVG29 was observed by transmission electron microscopy (TEM, H-600, Hitachi, Japan) with 2% aqueous phosphotungstic acid staining.

The amounts of NBP and DA were measured using high-performance liquid chromatography (HPLC, Supplementary Information). The drug loading capacity (DL) and entrapment efficiency (EE) were calculated using the following formulas:

$$EE\% = (\text{weight of loaded drug}/\text{weight of feeding drug}) \times 100\%$$

$$DL\% = (\text{weight of loaded drug}/\text{total weight of liposomes}) \times 100\%$$

To investigate the stability of liposomes, Lips, Lips-RVG29, (NBP+DA)-Lips and (NBP+DA)-Lips-RVG29 mixed with PBS were placed at 4 °C, 25 °C, and 37 °C.[27] Changes in particle size were recorded over time (1, 2, 3, 4, 5, 6 and 7

d). Moreover, the variation in the absorbance of the liposomes was monitored at 37 °C for 48 h to evaluate their serum stability in the presence of FBS. The absorbance (A) at different time points was measured using a microplate reader at 750 nm, and the transmittance (T) was converted based on absorbance (A): ($T\% = 10^{-A}$).[28]

In vitro Drug Release Study

The in vitro release behavior of NBP and DA from liposomes was investigated using the dialysis method.[29] Briefly, an aliquot of free NBP+DA, (NBP+DA)-Lips, (NBP+DA)-Lips-RVG29, NBP-Lips-RVG29 and DA-Lips-RVG29 were added into dialysis bags (MWCO 3500 Da). The dialysis bags were immersed in 40 mL of PBS (pH 7.4) and incubated at 37 °C under constant shaking at 100 rpm. At predetermined time points (0.25, 0.5, 1, 2, 4, 6, 8, 10, 12, 24, 36, 48 and 72 h), 0.1 mL of the external medium was sampled and replaced with an equal volume of fresh PBS. The released NBP and DA in the medium were measured by the liquid chromatography-tandem mass spectrometry (LC-MS/MS, Supplementary Information, Table S1).

The Level of nAChR Expression of Three Cell Lines

The level of nAChR expression of three cell lines (PC12, bEnd.3 and JAWSII cells) was measured by Western blotting as described.[30] When reaching 80–90% confluence, cells were collected to make whole cell lysates with RIPA lysis buffer (Beyotime, Haimen, China). The content of total protein in each group was measured by the Micro BCA Protein Assay Kit. Next, the samples containing equal amounts of protein were analyzed by SDS-PAGE and transferred onto a nitrocellulose membrane. The membranes were incubated with mouse anti-β-actin antibody (sc-81178, Santa Cruz Biotechnology, Dallas, Texas, USA) or rabbit anti-AChR antibody (No. A9808 and A0350, ABclonal, Wuhan, China) at 4 °C overnight, and then incubated with horseradish peroxidase-labeled goat anti-rabbit IgG (No. AS014, ABclonal, Wuhan, China) at room temperature for 1 h. The proteins were detected on a ChemiDoc MP System (Bio-Rad, USA) by Immobilon Western HRP Substrate (Millipore, Massachusetts, USA).

Cellular Uptake of Liposomes in PC12 Cells

The PC12 cells were seeded in 12-well plates (1×10^5 cells/well). When the cells grew up to 80–90% confluence, DiD-Lips and DiD-Lips-RVG29 were added into the plates at a final DiD concentration of 400 ng/mL. Cells were incubated for 1, 2, 4, 8, 12 and 24 h at 37 °C, respectively. Then, the cells were washed thrice with ice-cold PBS, trypsinized and resuspended in PBS. Finally, the fluorescence intensity of the cells was recorded using a flow cytometer (Cytomics™ FC 500, Beckman Coulter, USA). PC12 cells were pre-incubated with RVG29 (400 μg/mL) to explore the uptake mechanism. The cellular uptake by bEnd.3 cells and JAWSII cells was studied as a positive or negative control. To study the effects of temperature and energy inhibitors, PC12 cells were treated with DiD-Lips-RVG29 for 1 h at 4 °C or were pretreated with sodium azide (NaN_3, 1 mg/mL) for 30 min. Moreover, inhibitors including chlorpromazine (clathrin inhibitor, 10 μg/mL), amiloride (acid-sensing ion channel inhibitor, 20 μg/mL), nystatin (caveolin inhibitor, 25 μg/mL) and cytochalasin D (actin microfilament inhibitor, 1 μg/mL) were also investigated.

Cellular uptake of Lips-RVG29 was also evaluated by confocal laser scanning microscopy (CLSM, FV1000, Olympus, Japan). After incubation with DiD, DiD-Lips and DiD-Lips-RVG29 for 1 h, PC12 cells were washed with PBS and fixed with 4% paraformaldehyde for 15 min. Next, the cytoskeleton and nuclei were stained with FITC-labelled phalloidin for 30 min and DAPI for 5 min, respectively. Finally, the cells were viewed using a CLSM. Meanwhile, a group of PC12 cells were pre-incubated with free RVG29 for 30 min and then treated as described above.

In vivo BBB Penetration Ability of Liposomes in a bEnd.3 Cells-Based BBB Model

For transendothelial transport experiments, an in vitro BBB model was established using bEnd.3 cells according to the report.[31] Briefly, the cells (1×10^5 cells/well) were seeded onto the upper chamber of the transwell (Corning, NY, USA). After incubation for 7 days, a tight and compact monolayer was formed. Then, the permeability of the model was measured by using sodium fluorescein (a BBB impermeable dye). In brief, transwell inserts with or without bEnd.3 cells were treated with 0.5 mL sodium fluorescein solution (2 μg/mL) and the basal compartment were given 1.5 mL Ringer-HEPES buffer. At the indicated time points (0.25, 0.5, 1, 1.5, 2, 3, 4, 5 and 6 h), 200 μL buffer was taken out from the

basal compartment, and an equal volume of fresh Ringer-HEPES buffer was added. The samples were analyzed using a microplate reader at 493 nm to determine the fluorescence intensity and the leakage ratio of sodium fluorescein was calculated.

Subsequently, the transendothelial transport of liposomes was analyzed using a bEnd.3-based BBB model. Briefly, 0.5 mL (NBP+DA)-Lips or (NBP+DA)-Lips-RVG29 was added to the apical side of the insert at a total drug concentration of 60 μg/mL, and 1.5 mL Ringer-HEPES buffer was added to the basal compartment. At the indicated time points (0.25, 0.5, 1, 1.5 and 2 h), 200 μL buffer was collected from the basal compartment, and the same volume of fresh Ringer-HEPES buffer was added. The samples were analyzed using LC-MS/MS to determine the drug concentration and the cumulative infiltration volume (total amount of drug accumulated in the basal compartment/initial drug concentration in the upper chamber) and apparent permeability coefficient (P_{app}) of the liposomes were calculated.[32–34] Meanwhile, the transportation of (NBP+DA)-Lips-RVG29 was also investigated at 4 °C.

In vitro Therapeutic Efficacy of Liposomes in 6-OHDA-Induced PC12 Cells

The neuroprotective effects of (NBP+DA)-Lips-RVG29 were investigated in 6-OHDA-induced PC12 cells. PC12 cells were seeded in 96-well culture plates (2×10^4 cells/well) and 12-well culture plates (1×10^5 cells/well). When cells grew up to 80–90% confluence, the cells were treated with serum- and antibiotics-free medium (control), free NBP+DA, (NBP+DA)-Lips, (NBP+DA)-Lips-RVG29, DA-Lips-RVG29 and NBP-Lips-RVG29, and the final concentration of NBP or/and DA was 100 μM. After 2 h incubation, 6-OHDA was added at a final concentration of 100 μM and cells were incubated for another 24 h. The cell viability, cell apoptosis and ROS levels were determined as described in Section "Synergistic effects of NBP and DA". Meanwhile, the cells were collected, lysed using freeze-thaw cycles, centrifuged at 10000 rpm for 10 min at 4 °C to obtain the supernatant after the treatment. Oxidative stress-related biomarkers including superoxide dismutase (SOD), reduced glutathione (G-SH), catalase (CAT), antioxidant capacity (T-AOC), and inflammatory cytokines including interleukin-6 (IL-6), interleukin-1β (IL-1β), tumor necrosis factor-α (TNF-α) were estimated by quantitative analysis using commercial reagent kits (Solarbio, Beijing, China).

Pharmacokinetics Study of Liposomes in Sprague-Dawley Rats

SD rats were randomly divided into 3 groups (n = 5). Free NBP+DA, (NBP+DA)-Lips and (NBP+DA)-Lips-RVG29 were administered intravenously at a total drug dosage of 32 mg/kg. Then, the blood samples (approximately 0.3 mL) were obtained via the orbital venous plexus at scheduled time points (0.083, 0.25, 0.5, 1, 2, 4, 8, 12 and 24 h). All blood samples were immediately centrifuged at 6000 rpm for 5 min to obtain the plasma supernatants. The drug concentrations in different plasma samples were determined by LC-MS/MS.

In vivo Biodistribution of Liposomes in Mice

Mice were randomly divided into 3 groups (n = 18) and intravenously administered with free DiD, DiD-Lips or DiD-Lips-RVG29 at an equivalent dose of 200 μg DiD/kg. Mice were sacrificed to collect the major organs (heart, liver, spleen, lung, kidney and brain) at 0.5, 1, 2, 4, 8 and 24 h after administration. Then, the organs were washed with saline and dried with filter paper for ex vivo imaging study.

To further investigate the distribution of liposomal drugs in vivo, mice were randomly divided into 3 groups (n = 5) and intravenously administered with free NBP+DA, (NBP+DA)-Lips or (NBP+DA)-Lips-RVG29 at a total drug dosage of 40 mg/kg. Mice were sacrificed at 1 h after administration. The major organs were collected, weighed and homogenized with two folds of PBS (g/mL). The concentrations of NBP and DA in the different organs were determined by LC-MS/MS.

In vivo Targeting Ability of Liposomes to Brain Lesions Area of PD

To verify the brain lesions area-targeting ability of (NBP+DA)-Lips-RVG29, the mice were intravenously injected with free DiD, DiD-Lips or DiD-Lips-RVG29 (200 μg DiD/kg). The mice were sacrificed at 1 h after administration. The whole brains were isolated and fixed in 4% paraformaldehyde for 48 h. Next, the brain samples were gently washed with cold normal saline, frozen at −80 °C in cryoembedding media (Sakura, Torrance, CA, USA) and sectioned at 10 μm

thickness (MEV, SLEE, Germany). The sections were then fixed with 4% buffered paraformaldehyde and sequentially stained with DAPI. Finally, the sections of striatum, substantia nigra and hippocampus were imaged by CLSM.

In vivo Therapeutic Efficacy of Liposomes in a 6-OHDA-Induced Mouse Model of PD

The 6-OHDA-induced mouse model of PD was established as described previously.[33,35] The model mice were randomly divided into six groups (n = 15) and treated respectively with normal saline, NBP+DA, (NBP+DA)-Lips, (NBP+DA)-Lips-RVG29, DA-Lips-RVG29 and NBP-Lips-RVG29 (the dosage of NBP or/and DA was 26 μmol/kg) via tail vein injection per 2 days for 10 times. Another sham group was injected with saline in a similar manner and served as the control group. After 21 days, all mice were sacrificed after behavioral tests, and the brains were harvested for immunohistochemical staining of tyrosine hydroxylase (TH) and α-Syn expression, LC-MS/MS detection of DA, and assessment of enzymatic antioxidants and inflammatory factors.

To evaluate the effect of (NBP+DA)-Lips-RVG29 on the impairment of motor function in the 6-OHDA-induced PD mouse model, we performed pole test and exploratory behavior test. The pole test was performed according to previously published methods with minor modifications.[36] Briefly, the mouse was placed on the top of a rough-surfaced vertical wooden pole (0.8 mm in diameter, 60 cm in height) with their head facing upside. The time required for the mouse to reach the bottom of the pole was recorded. If the mouse did not reach the bottom in 5 min, it was guided and the time was recorded as 5 min. Based on previous studies, the exploratory behavior test was conducted with minor modifications.[36] The test consisted of a polyvinyl chloride (PVC) box as the square arena (42 × 42×42 cm). The mouse was placed in the center of the arena and acclimatized for 10 min, and the number of rearing within 5 min was recorded.

Then, the mice were sacrificed and the lesioned right striatum tissues were quickly collected and stored at −40 °C for subsequent assays. The level of lesioned striatal DA was determined using LC-MS/MS. Briefly, each striatum was homogenized with two folds of normal saline (1% formic acid), and then diluted with acetonitrile. Homogenates were vortexed for 3 min and centrifuged at 13400 rpm for 10 min at 4 °C. The supernatants were analyzed by LC-MS/MS.[25]

Afterwards, The TH activity and α-Syn level in lesioned striatum tissues were evaluated by immunohistochemical staining. The lesioned brains were removed and kept in 4% paraformaldehyde overnight. Next, the brains were embedded in paraffin and serially cut using a cryotome. The sections were incubated with anti-TH (No. 25859-1-ap, Proteintech Group Inc., Chicago, USA) or anti-α-Syn antibody (No. ab212184, Abcam, Cambridge, UK), subsequently with biotinylated Goat Anti-Rabbit IgG (No. ab205718, Abcam, Cambridge, UK). Finally, photomicrographs were obtained using a microscope camera (Eclipse 80i, Nikon, Japan). Moreover, the expression level of α-Syn in the lesioned brain was further investigated by Western blotting.

Finally, the lesioned striatum tissues were collected, homogenized with two folds of normal saline. The mixture was centrifuged at 8000 rpm for 10 min at 4 °C. The level of oxidative stress-related biomarkers (SOD, G-SH, CAT and T-AOC) and inflammatory cytokines (IL-6, IL-1β and TNF-α) in the supernatants were measured using reagent kits (Solarbio) according to the manufacturer's instructions.

Safety Evaluation of Liposomes in Mice

The mice were randomly divided into six groups (n = 5) and injected intravenously with normal saline, free NBP+DA, (NBP+DA)-Lips, (NBP+DA)-Lips-RVG29, DA-Lips-RVG29 and NBP-Lips-RVG29 (the dosage of NBP or/and DA was 26 μmol/kg) per 2 days for 10 times, respectively. After 21 days, blood samples and major organ tissues (heart, liver, spleen, lung, kidney and brain) of the mice were collected. White blood cells (WBC), red blood cells (RBC) and platelets (PLT) were counted using an MEK-6318K Automated Hematology Analyzer (Nihon Kohden, Shinjuku-ku, Japan). The levels of alanine aminotransferase (ALT), aspartate aminotransferase (AST), creatinine kinase MB isoenzyme (CK-MB), lactate dehydrogenase (LDH), uric acid (UA) and urea nitrogen (BUN) in serum were measured by Hitachi 7020 automatic biochemical analyzer (Hitachi, Japan). The main organs were fixed with 4% paraformaldehyde and stained with hematoxylin and eosin (H&E) for histological analysis.

Statistical Analysis

Statistical analysis was performed using the GraphPad Prism software (version 6.01). Statistical significances were assessed using Student's *t*-test and one-way ANOVA. Data averages were presented as means ± standard deviation (SD). The significance was defined as follows: $*p < 0.05$, $**p < 0.01$ and $***p < 0.001$.

Results and Discussion

The synergistic effects of NBP and DA were tested by MTT assay, ROS measurement and cell apoptosis assay in 6-OHDA-induced PC12 cells. The effect of different concentrations of 6-OHDA on the viability of PC12 cells was investigated to select the appropriate modeling concentration for subsequent studies. Referring to the value of IC_{50}, the final optimized 6-OHDA concentration was 100 μM (Figure 1A).

As shown in Figure 1B, the cell viability of PC12 cells remarkably reduced after incubation with 100 μM 6-OHDA. After treatment with different proportions of NBP and DA, the cell survival rates improved to varying degrees. Similarly, 6-OHDA treatment alone induced a significant increase in apoptosis level (Figure 1C and D) and ROS level (Figure 1E) compared with the control group, while various combination treatments of NBP and DA decreased the apoptosis and ROS level. In general, NBP and DA showed the effective synergistic protective effect against 6-OHDA-induced cell injury compared to monotherapy. More importantly, the effect of NBP:DA ratio 1:1 (mol/mol) was the strongest among all. Therefore, the molar ratio of NBP:DA 1:1 was chosen to carry out the following studies.

(NBP+DA)-Lips-Mal was successfully prepared by the thin-film hydration and sonication method. Then, RVG29-Cys was conjugated to DSPE-PEG2000-Mal by the post-insertion method to obtain (NBP+DA)-Lips-RVG29. Tricine-SDS-PAGE result confirmed the successful coupling between RVG29 and DSPE-PEG2000-Mal (Figure 2A). The excess free peptide was removed using a Sepharose CL-4B spun column (Solarbio). The coupling rate of RVG29 was 97.40 ± 0.01%, and the modification density of RVG29 on the liposomes surface was approximately 0.036 ± 0.005 (proteins/phospholipids, mol/mol).

The particle size, PDI and zeta potential of the different formulations were shown in Figure 2B–D. (NBP+DA)-Lips displayed an average size of 115.4 ± 1.08 nm and a negative zeta potential of −29.3 ± 0.62 mV. (NBP+DA)-Lips-RVG29 showed an average particle size of 129.5 ± 2.00 nm and a negative zeta potential of −26.6 ± 0.53 mV. Compared with unmodified liposomes, (NBP+DA)-Lips-RVG29 had a slightly increased particle size and zeta potential. However, there was no obvious change in the particle size of liposomes before and after drug loading. The TEM image of (NBP+DA)-Lips-RVG29 showed a roughly spherical shape and typical bilayer structure (Figure 2D). The coupling of RVG29 had few effect on the encapsulation and loading efficiency of NBP and DA. The encapsulation efficiencies of NBP and DA in (NBP+DA)-Lips-RVG29 were determined as 65.02 ± 0.009% and 61.60 ± 0.011%, respectively. The total loading capacity was 3.95 ± 0.009%.

We explored the in vitro stability of liposomes by monitoring their particle size and absorbance variation. In PBS, none of the formulations (Lips, Lips-RVG29, (NBP+DA)-Lips and (NBP+DA)-Lips-RVG29) showed drastic changes in particle size after seven days at 4 °C, 25 °C, and 37 °C (Figures 2E and S1A and B). It is well known that the activity of therapeutic agent would be influenced by the stability of carriers under biological environment, so the stability of liposomes was investigated in 50% FBS as well.[37] The drug carriers could bind to serum albumins because the absorbance variation increased slightly after incubation with FBS for 48 h (Figure S1C). However, the light transmittance of all the liposomes were hardly changed, suggesting that the liposomes were still stable (Figure 2F).

Figure 2G and H showed the in vitro release profiles of free NBP+DA, (NBP+DA)-Lips, (NBP+DA)-Lips-RVG29, NBP-Lips-RVG29 and DA-Lips-RVG29. Compared with the rapid release of free NBP and DA, liposomes showed more sustained release patterns with no burst release of the loaded drugs. After 12 h, approximately 80–90% cumulative release was observed for free NBP+DA, whereas approximately 40% cumulative release percentage was achieved by liposomes. Moreover, there was no significant difference in release behavior among (NBP+DA)-Lips, (NBP+DA)-Lips-RVG29, NBP-Lips-RVG29 and DA-Lips-RVG29 at each time point. The above results indicated that the modification of RVG29 did not affect the release properties of NBP and DA in liposomes, and the two drugs did not affect the release profile of each other either.

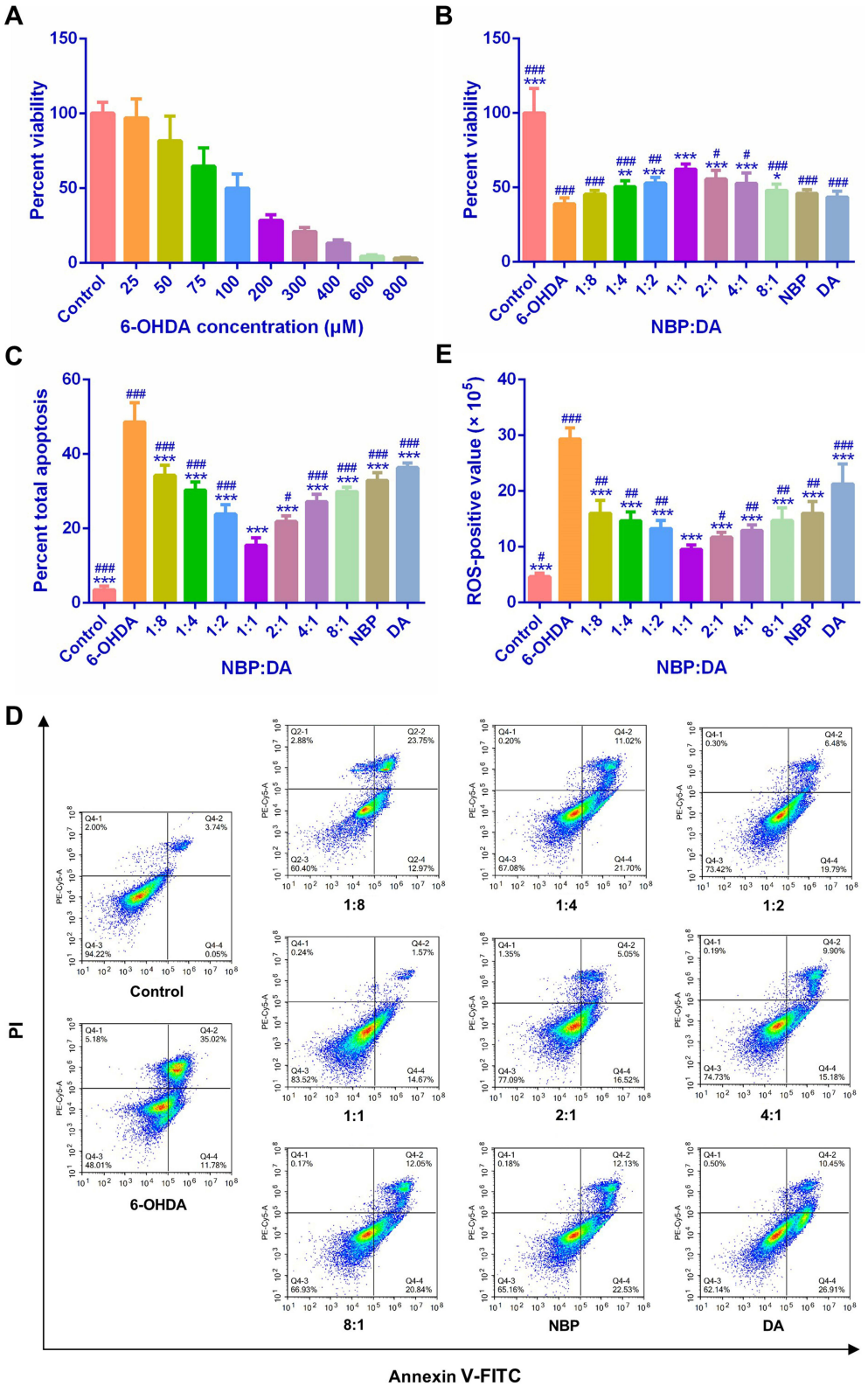

Figure 1 Synergistic effects of NBP and DA in a 6-OHDA-induced cellular model of PD. (**A**) Cell viability of PC12 cells after 24 h incubation with 6-OHDA at varied concentrations (mean ± SD, n = 6). (**B**) Cell viability of 6-OHDA-induced PC12 cells after 24 h incubation with NBP and DA at varied molar rations (mean ± SD, n = 6). (**C**) Proportion of apoptotic cells after different treatments (mean ± SD, n = 4). (**D**) Apoptosis assays conducted by flow cytometry. (**E**) ROS levels in 6-OHDA-treated PC12 cells after 24 h incubation with NBP and DA at varied molar rations (mean ± SD, n = 4). *$p < 0.01$, **$p < 0.01$ and ***$p < 0.001$ vs 6-OHDA group. $^{\#}p < 0.01$, $^{\#\#}p < 0.01$ and $^{\#\#\#}p < 0.001$ vs ratio 1:1.

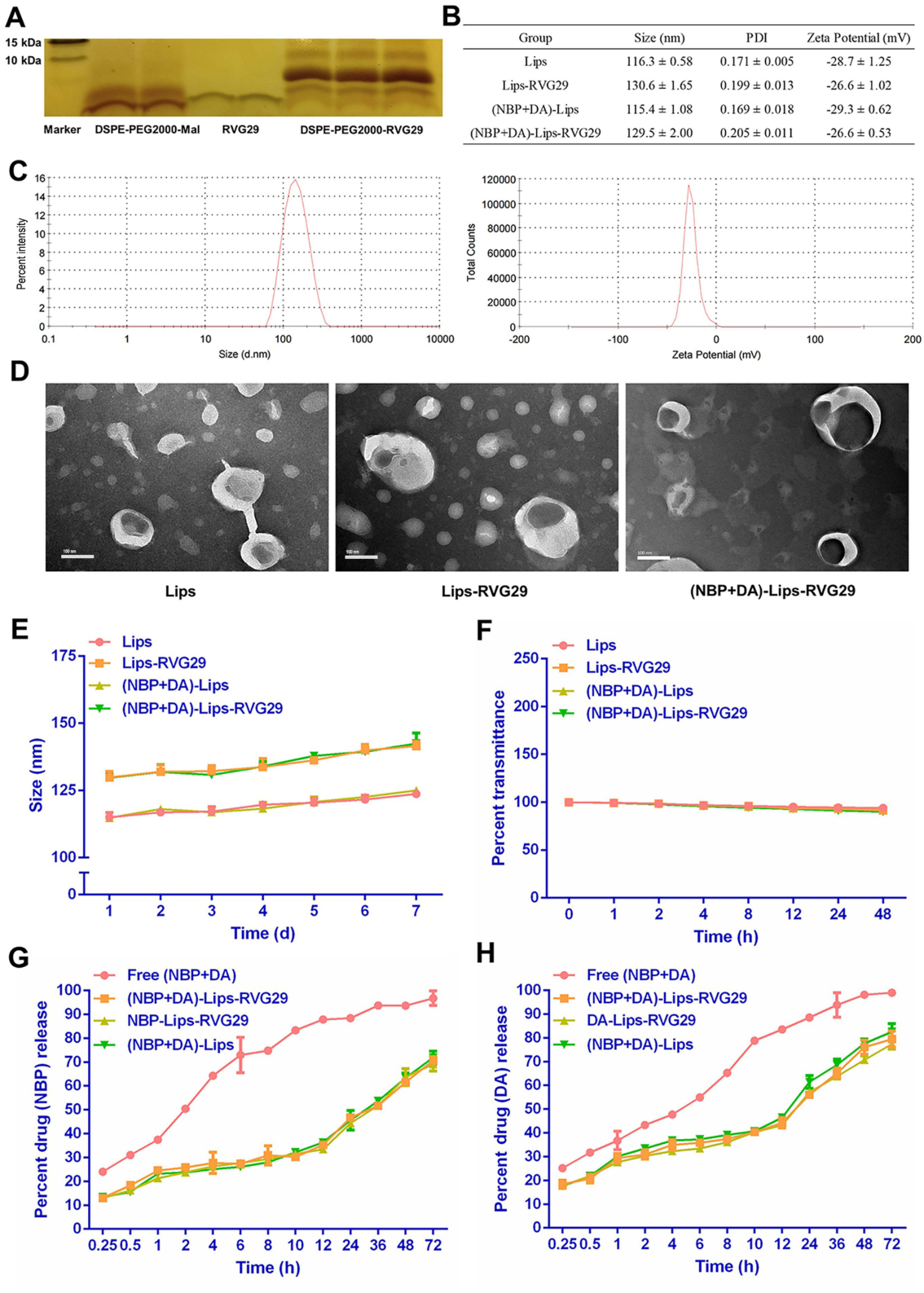

Group	Size (nm)	PDI	Zeta Potential (mV)
Lips	116.3 ± 0.58	0.171 ± 0.005	-28.7 ± 1.25
Lips-RVG29	130.6 ± 1.65	0.199 ± 0.013	-26.6 ± 1.02
(NBP+DA)-Lips	115.4 ± 1.08	0.169 ± 0.018	-29.3 ± 0.62
(NBP+DA)-Lips-RVG29	129.5 ± 2.00	0.205 ± 0.011	-26.6 ± 0.53

Figure 2 Characterization of prepared liposomal carriers. (**A**) The Tricine-SDS-PAGE analysis of the coupling between RVG29 (3.37 kDa) and DSPE-PEG2000-Mal (2.96 kDa). (**B**) Particle size, PDI and zeta potential of liposomes (mean ± SD, n = 3). (**C**) Representative size distribution graph and zeta potential distribution graph of (NBP+DA)-Lips-RVG29. (**D**) TEM images of liposomes. Scale bar: 100 nm. (**E**) The particle size variation of liposomes in PBS at 37 °C for 7 days. (**F**) Transmittance variation of liposomes in FBS for 48 h (mean ± SD, n = 3). (**G** and **H**) Drug release behaviors of free NBP+DA and liposomes in 50% PBS for 72 h (mean ± SD, n = 3).

The PC12 cells, exhibiting the properties of dopaminergic cells, were widely used as an in vitro cellular model of PD.[38] The bEnd.3 cells, exhibiting the properties of endothelial, were usually used to construct in vitro BBB models.[39] The expression level of nAChR by the two cells were investigated using Western blotting. Meanwhile, murine dendritic cell line JAWS II was used as a negative control. Both PC12 and bEnd.3 cells exhibited high level of AChR α4 and AChR β2 expression, while low level expression of nAChR was detected by JAWS II cells (Figure 3A). The results indicated that (NBP+DA)-Lips-RVG29 had the potential to cross the BBB and even reach the diseased neurons by binding to nAChR, thereby realizing the synergistic anti-PD effect of NBP and DA.

DiD-Lips-RVG29 was incubated with PC12 cells to investigate the cellular uptake. As shown in Figure 3B, the fluorescence intensity of PC12 cells treated with DiD-Lips-RVG29 was much higher than these treated with DiD-Lips at each time point tested, whereas the fluorescence intensity in the Lips-RVG29 group was significantly decreased with pre-incubation of free RVG29. Similar results were observed from the CLSM images of the PC12 cells (Figure 3C) and the cellular uptake of bEnd.3 cells (Figure 3D). However, free RVG29 did not affect the cellular uptake efficiency of Lips-RVG29 by JAWSII cells (Figure 3D). These above results were unsurprising, because PC12 cells and bEnd.3 cells have high nAChR expression level compared with JAWSII cells, which could be recognized by RVG29. These results indicated that the cellular uptake of Lips-RVG29 was mediated by the specific binding between RVG29 and nAChR.

We further explored the internalization mechanism of Lips-RVG29 by blocking specific endocytosis pathways with various inhibitors. The fluorescence intensity of PC12 cells treated with DiD-Lips-RVG29 was significantly decreased at 4 °C or with pre-incubation of NaN_3, revealing that the uptake of Lips-RVG29 was an active and energy-dependent process (Figure 3E). Meanwhile, chlorpromazine, amiloride, nystatin and cytochalasin D significantly decreased the uptake efficiency (Figure 3E), indicating that clathrin, acid-sensing ion channels, caveolin and micropinocytosis mediated the internalization of Lips-RVG29 to varying degrees.

The BBB penetration of Lips-RVG29 was investigated using a bEnd.3 cells-based BBB model. The integrity of the monolayer was observed by measuring the transendothelial electrical resistance (TEER) and the leakage ratio of sodium fluorescein.[34] The minimum TEER value of a complete membrane was 250 $\Omega \cdot cm^2$, while the TEER was up to 360 ± 5 Ω·cm after incubation for 7 days. Moreover, sodium fluorescein quickly passed through the blank membrane, and the leakage percentage of sodium fluorescein (94.98%) was much higher than that in the BBB model group (33.97%) within 6 h (Figure 3F). These results confirmed the successful establishment of the BBB model. Afterwards, the above model was used to investigate the BBB penetration of (NBP+DA)-Lips-RVG29 in vitro. As shown in Figure 3G and H, the accumulated cleared volumes of all groups were continuously increased over time, and the accumulated cleared volume of drugs in (NBP+DA)-Lips-RVG29 was much higher than that of (NBP+DA)-Lips at each time point. After 2 h incubation at 37 °C, the P_{app} of NBP and DA in (NBP+DA)-Lips were (2.35 ± 0.159) × 10^{-7} cm/s and (2.35 ± 0.351) × 10^{-7} respectively, whereas the P_{app} of NBP and DA in (NBP+DA)-Lips-RVG29 were (4.31 ± 0.341) × 10^{-7} cm/s and (4.45 ± 0.200) × 10^{-7} respectively (Figure 3I). These results suggested that (NBP+DA)-Lips-RVG29 could cross the BBB more easily. In addition, the P_{app} of NBP and DA in (NBP+DA)-Lips-RVG29 was significantly reduced to (1.77 ± 0.246) × 10^{-7} cm/s and (1.71 ± 0.265) ×10^{-7} cm/s at 4 °C, indicating that the transport of (NBP+DA)-Lips-RVG29 across the BBB requires energy.

The in vitro neuroprotective effects of (NBP+DA)-Lips-RVG29 were explored using a 6-OHDA-induced cellular model of PD. As shown in Figure 4A, 100 μM 6-OHDA treatment reduced the viability of PC12 cells to 42.0% of the control, while all treatments have improved cell viability. Notably, the (NBP+DA)-Lips-RVG29 group showed the most significant improvement in the survival rate, reaching 74.3%.

The effect of (NBP+DA)-Lips-RVG29 on 6-OHDA-induced apoptosis was analyzed using Annexin V-FITC/PI staining. The percentage of apoptotic cells was obtained by calculating the sum of early and late apoptosis rates.[40] After exposing PC12 cells to 6-OHDA, the apoptosis percentage was up to 44.1% (Figure 4B and C). After treatment with (NBP+DA)-Lips-RVG29, the apoptotic cell percentage was reduced significantly to 10.6%. This reduction extent was greater than that observed in other groups.

Oxidative stress plays an important role in the neurodegenerative pathogenesis of PD.[41] We found that (NBP+DA)-Lips-RVG29 could inhibit the formation of ROS in 6-OHDA-treated PC12 cells more strongly than other groups (Figure 4D). SOD, G-SH, CAT and T-AOC are well known biomarkers of oxidative stress.[42,43] SOD is a class of

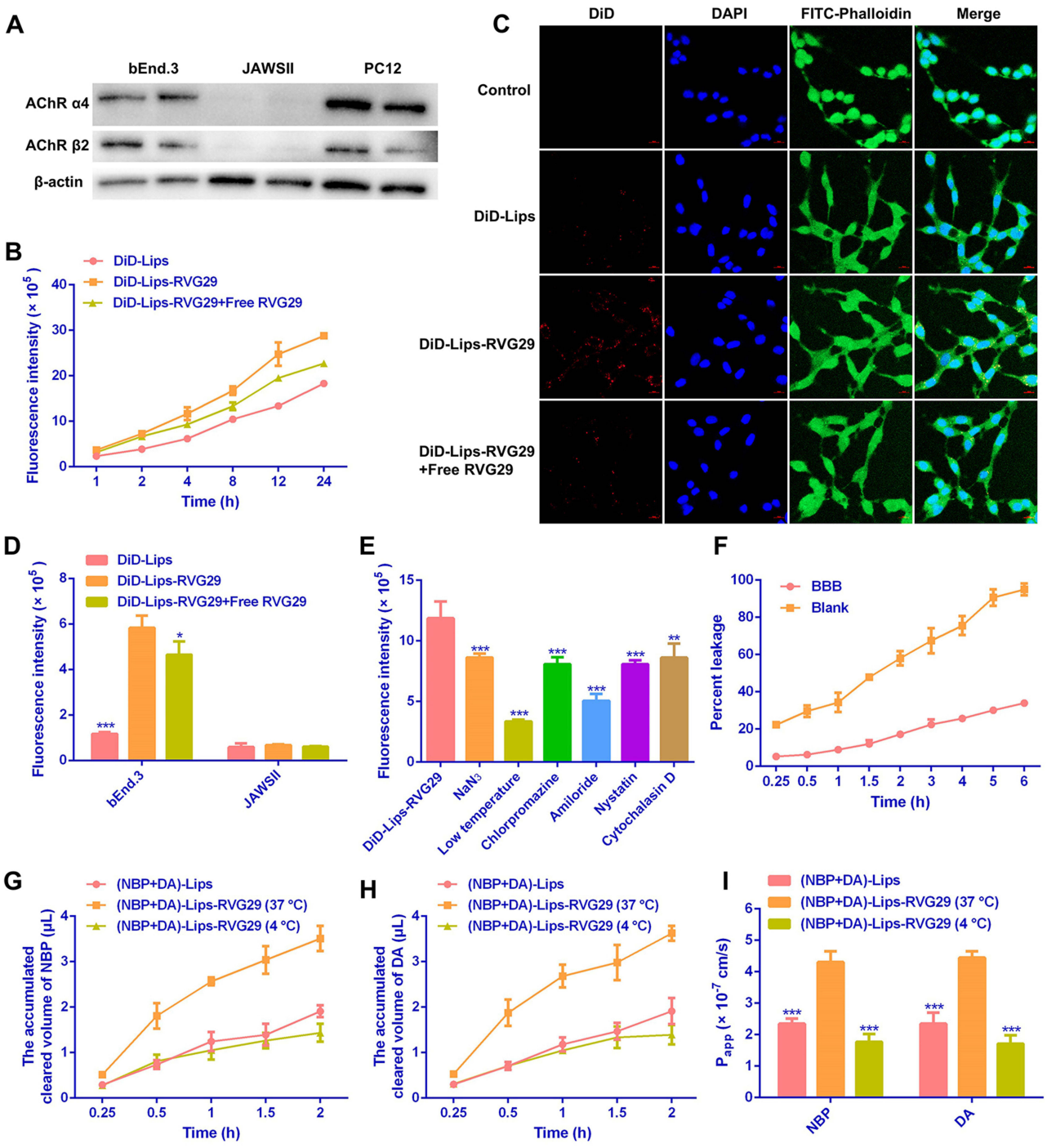

Figure 3 In vitro brain targeting of Lips-RVG29. (**A**) The level of AChR α4 (70 kDa) and AChR β2 (57 kDa) expression by Bend.3 cells, PC12 cells and JAWSII cells (β-actin: 42 kDa). (**B**) The cellular uptake of liposomes by PC12 cells at different time points (mean ± SD, n = 3). (**C**) CLSM images of PC12 cells incubated with liposomes for 1 h. The nuclei were stained with DAPI (blue), cell membranes were stained with FITC-labeled phalloidin (green) and liposomes were shown in red. Scale bar: 50 μm. (**D**) The cellular uptake of liposomes by bEnd.3 cells and JAWSII cells after 1 h incubation (mean ± SD, n = 3). (**E**) The effects of energy and inhibitors on cellular uptake of Lips-RVG29 by PC12 cells (mean ± SD, n = 3). (**F**) The leakage ratio of sodium fluorescein (mean ± SD, n = 3). (**G** and **H**) The accumulated cleared volume of liposomal (**G**) NBP and (**H**) DA in the BBB model (mean ± SD, n = 3). (**I**) The P_{app} of liposomal NBP and DA after incubation on the BBB model for 2 h (mean ± SD, n = 3). *$p < 0.05$, **$p < 0.01$ and ***$p < 0.001$ vs DiD-Lips-RVG29 or (NBP+DA)-Lips-RVG29.

superoxide anion scavenging enzyme. G-SH could scavenge free radicals and peroxides. CAT is an important scavenging enzyme for H_2O_2, which is a toxic byproduct of aerobic metabolism. T-AOC is a crucial indicator of the antioxidant level. 6-OHDA induced downregulation of SOD, G-SH, CAT and T-AOC levels in PC12 cells (Figure 4E). As expected,

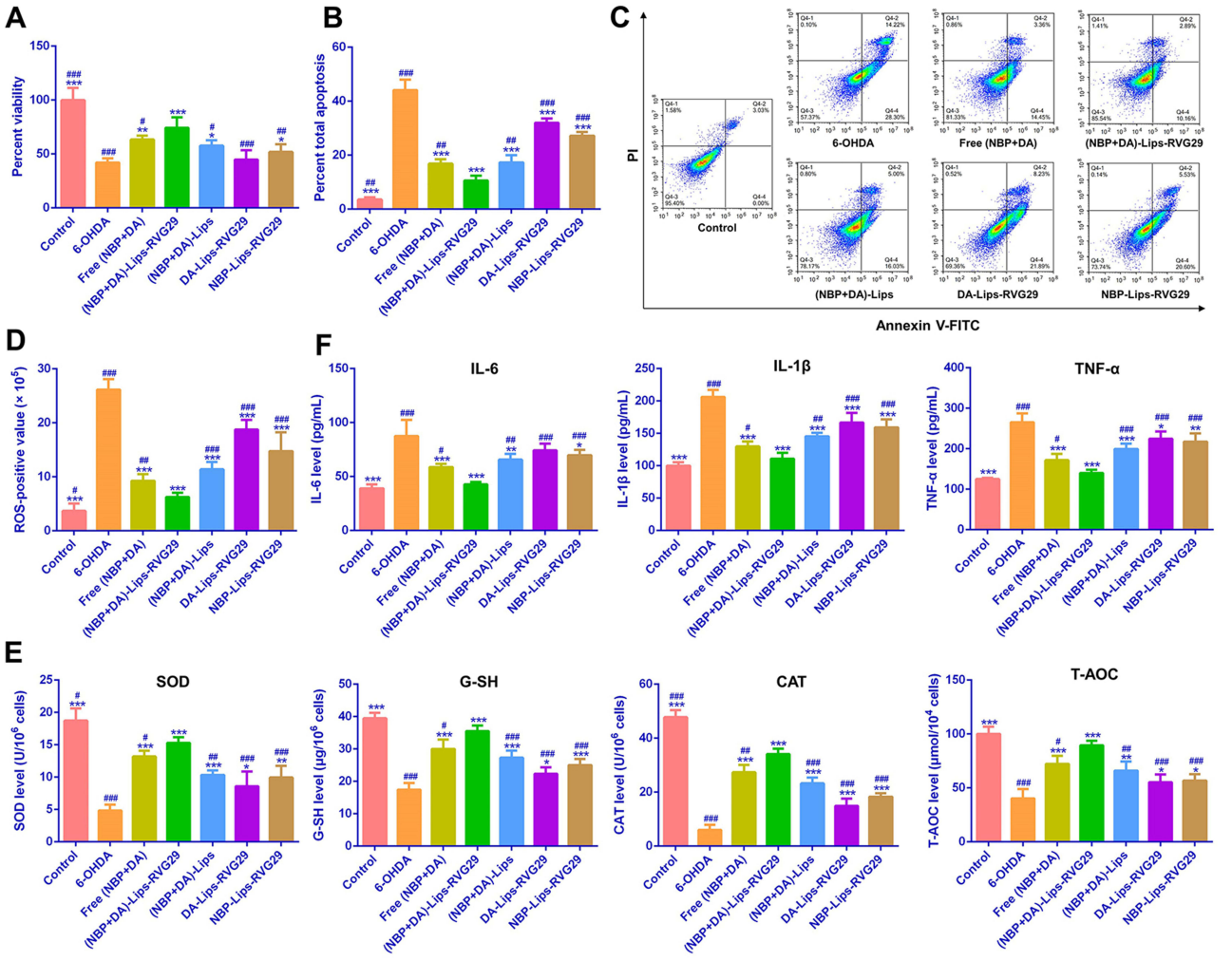

Figure 4 In vitro therapeutic effect of (NBP+DA)-Lips-RVG29 in a 6-OHDA-induced cellular model of PD. (**A**) Survival rate of PC12 cells after different treatments (mean ± SD, n = 6). (**B**) Apoptosis rate of PC12 cells after different treatments (mean ± SD, n = 4). (**C**) Apoptosis assay conducted by flow cytometry. (**D**) Cellular ROS level in PC12 cells after different treatments (mean ± SD, n = 4). (**E**) SOD, G-SH, CAT and T-AOC levels in PC12 cells after different treatments (mean ± SD, n = 4). (**F**) IL-6, IL-1β and TNF-α levels in PC12 cells after different treatments (mean ± SD, n = 4). $^{*}p < 0.01$, $^{**}p < 0.01$ and $^{***}p < 0.001$ vs 6-OHDA group. $^{\#}p < 0.01$, $^{\#\#}p < 0.01$ and $^{\#\#\#}p < 0.001$ vs (NBP+DA)-Lips-RVG29.

(NBP+DA)-Lips-RVG29 presented the strongest upregulation of these biomarkers among all treatments, showing powerful anti-oxidative ability.

Moreover, our results showed that the levels of inflammatory cytokines (IL-6, IL-1β and TNF-α) were significantly increased in PC12 cells after induction with 6-OHDA (Figure 4F). All of the treatments could reduce the level of inflammatory cytokines, while the anti-inflammatory ability of (NBP+DA)-Lips-RVG29 was more drastic than others.

These results further confirmed the superiority of the combination therapy of NBP and DA. More importantly, (NBP+DA)-Lips-RVG29 exhibited the greatest neuroprotective effects in the 6-OHDA-treated PC12 cells. These findings were consistent with the data presented in the cellular uptake assay.

A pharmacokinetic study was performed to investigate the in vivo circulation behavior of different liposomes. Free NBP and DA were quickly cleared from the systemic circulation (Figure 5A and B). Regarding the plasma pharmacokinetic parameters, the blood circulation half-life of liposomal NBP and DA was greatly extended compared to that of free drugs (Tables S2 and S3). Meanwhile, the plasma drug concentrations and the area under the plasma concentration-time curves of liposomal drugs were higher than those of free drugs as well. (NBP+DA)-Lips and (NBP+DA)-Lips-RVG29 showed similar pharmacokinetic profiles, and no significant differences were observed in their main

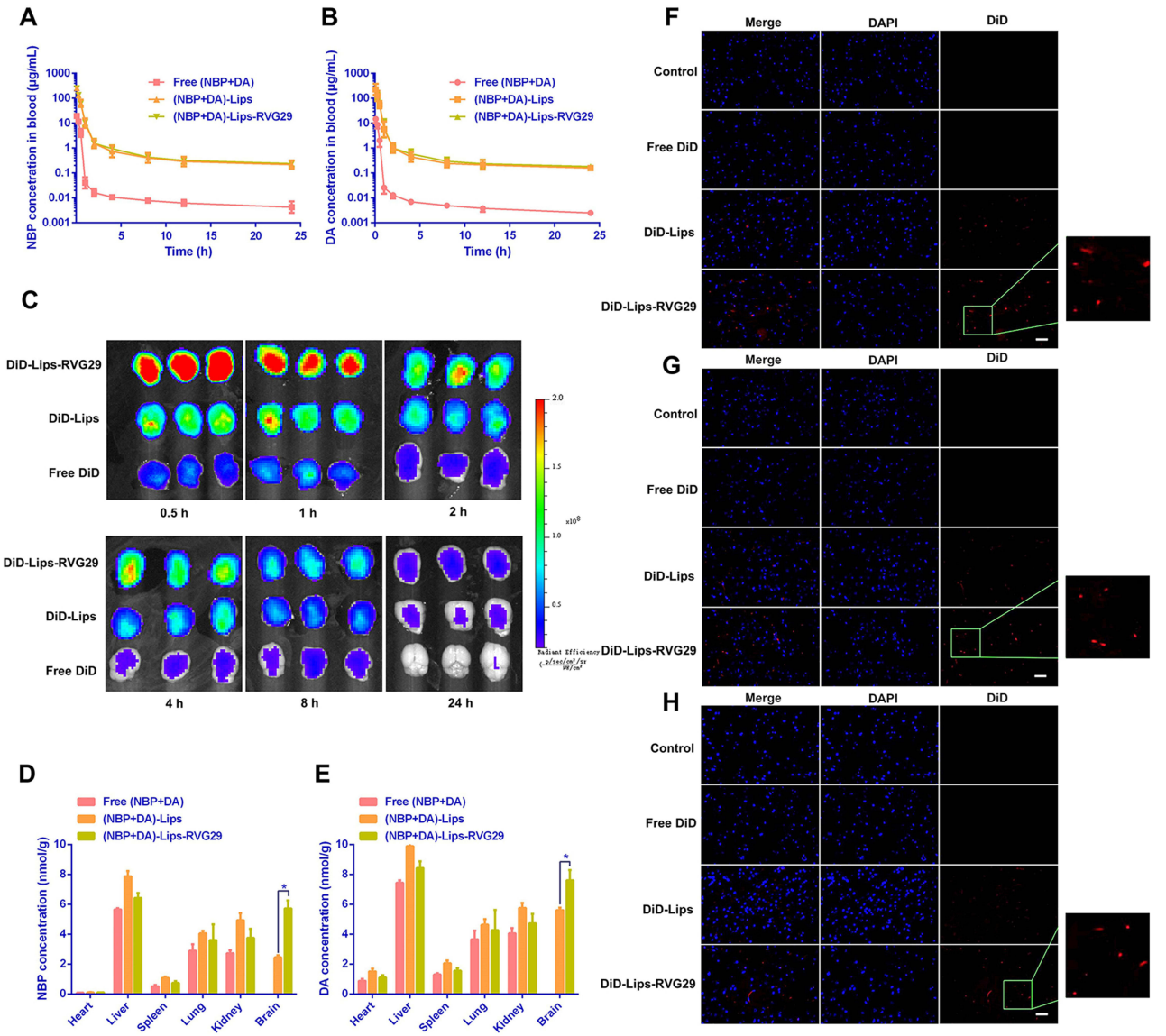

Figure 5 Evaluation of the in vivo brain targeting capacity of liposomes. (**A** and **B**) The concentration-time curves of NBP and DA in the blood after intravenous injection of free drugs, (NBP+DA)-Lips and (NBP+DA)-Lips-RVG29 (mean ± SD, n = 5). (**C**) Ex vivo brain images of mice at different time points post-injection of free DiD and DiD-labeled liposomes (mean ± SD, n = 3). (**D** and **E**) The concentration of NBP and DA in tissues at 1 h after intravenous injection of free drugs, (NBP+DA)-Lips and (NBP +DA)-Lips-RVG29 (mean ± SD, n = 5). *$p < 0.05$. (**F–H**) Fluorescence images of (**F**) striatum, (**G**) substantia nigra and (**H**) hippocampus in brain sections obtained at 1 h post-injection of free DiD and DiD-labeled liposomes. scale bar: 25 μm.

pharmacokinetic parameters ($p > 0.05$). Thus, the modification of RVG29 had little effect on the pharmacokinetic behavior of the liposomes. Additionally, the absorption behavior of NBP and DA in vivo was more consistent owing to co-encapsulation.

To verify the BBB-penetrating ability of Lips-RVG29 in vivo, mice were intravenously injected with DiD-labeled Lips-RVG29. The fluorescence intensity of DiD in the main organs was monitored using the near-infrared fluorescence imaging technique (Figure S2). As shown in Figure 5C, owing to the long circulation time, liposomes showed higher accumulation in the brain than free DiD. Importantly, mice injected with DiD-Lips-RVG29 exhibited extensive fluorescence in the brain during the observation period, whereas fewer fluorescence signals were detected in mice injected with unmodified liposomes. Therefore, these results indicated that Lips-RVG29 displayed a stronger ability to accumulate in the brain due to RVG29-mediated endocytosis.

The concentrations of NBP and DA in the brain were quantitatively analyzed using LC-MS/MS to further evaluate the brain targeting of Lips-RVG29 (Figure 5D and E). Unlike liposomes, free drugs could hardly cross the BBB. The brain distribution of NBP and DA in mice treated with (NBP+DA)-Lips-RVG29 was significantly higher ($p < 0.05$) than that in the (NBP+DA)-Lips group. On the contrary, compared with unmodified liposomes, the distribution of (NBP+DA)-Lips-RVG29 in other organs was slightly decreased. It's worth noting that the molar ratio of NBP and DA accumulated in the brain in (NBP +DA)-Lips-RVG29 group was closest to the optimal ratio, which was conducive to achieving synergistic therapeutic effects.

To explore whether Lips-RVG29 could reach the brain lesions area of PD after passing through the BBB, the distribution of liposomes in the striatum, substantia nigra and hippocampus was investigated by CLSM. As expected, extensive and distinct fluorescence signals of DiD in the frozen sections of the striatum, substantia nigra and hippocampus were observed in the DiD-Lips-RVG29 group (Figure 5F–H). In contrast, fluorescence in mice receiving free DiD or DiD-Lips was undetectable or relatively weak, suggesting a role for RVG29-mediated targeting. These results indicated that Lips-RVG29 could cross the BBB and further target the striatum, substantia nigra and hippocampus, achieving the co-delivery of NBP and DA to the diseased region of PD.

Owing to the enhanced distribution in the brain and the superior accumulation in the brain lesions area of PD, (NBP +DA)-Lips-RVG29 might have excellent efficacy in PD. A widely used unilateral 6-OHDA-induced mouse model of PD was established by direct injection of 6-OHDA into the medial forebrain bundle.[33,35] 6-OHDA-induced mice significantly prolonged the total time for climbing down the pole (18.31-fold of the control) and decreased the number of rearing (50% of the control) compared to the control (sham-operated) group, whereas all treatments significantly promoted 6-OHDA-induced mice to climb down the pole and increased the rearing number (Figure 6A and B). Notably, (NBP+DA)-Lips-RVG29 exhibited the greatest effect in attenuating behavioral defects, suggesting that (NBP +DA)-Lips-RVG29 could effectively reverse the behavioral deficiencies of PD mice.

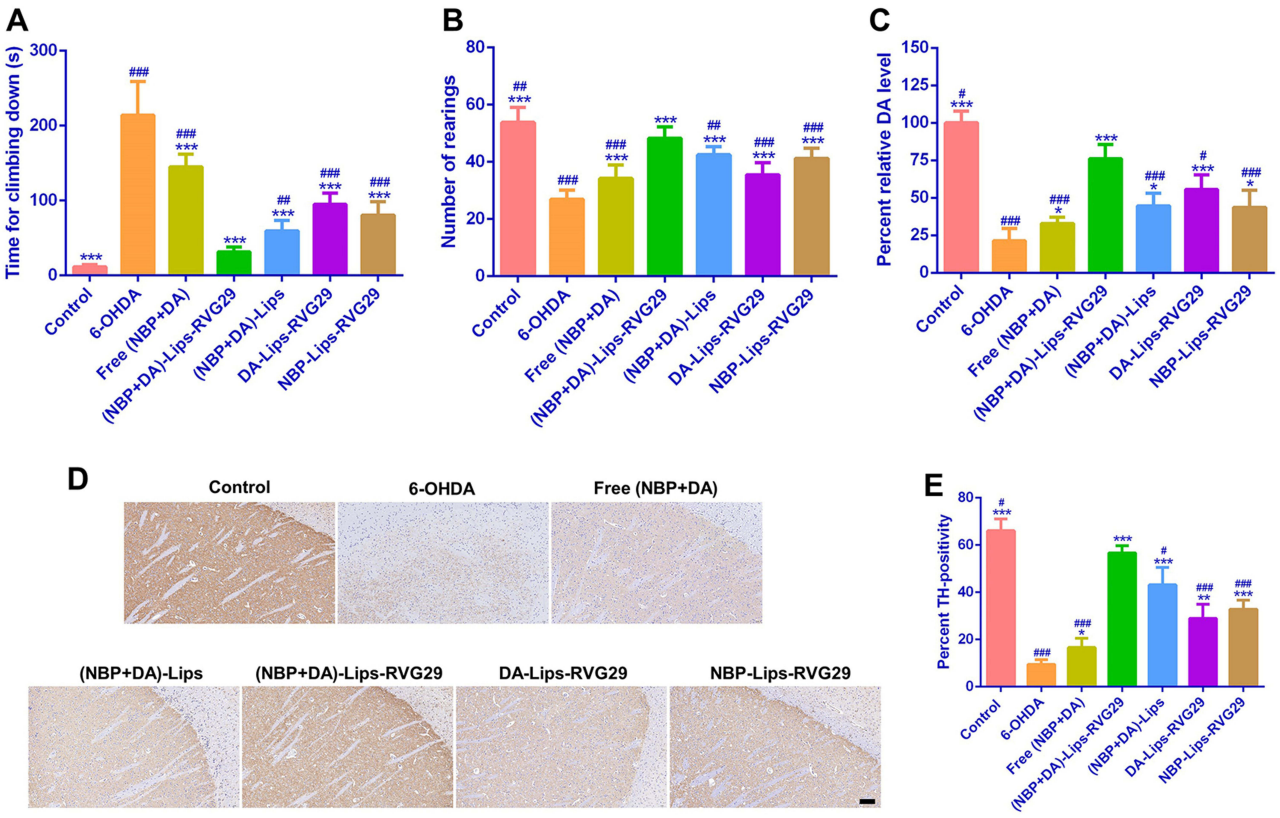

Figure 6 Therapeutic effect of (NBP+DA)-Lips-RVG29 on PD model mice. (**A**) Pole test (mean ± SD, n = 15). (**B**) exploratory behavior test (mean ± SD, n = 15). (**C**) DA percentage in the lesioned striatum of mice in different groups at 21 days after 6-OHDA lesion (mean ± SD, n = 4). (**D**) TH-immunoreactivity in the lesioned striatum of mice in different groups at 21 days after 6-OHDA lesion. scale bar: 100 μm. (**E**) The semi-quantitative analysis of TH-immunoreactivity (mean ± SD, n = 3). $^{*}p < 0.01$, $^{**}p < 0.01$ and $^{***}p < 0.001$ vs 6-OHDA. $^{\#}p < 0.01$, $^{\#\#}p < 0.01$ and $^{\#\#\#}p < 0.001$ vs (NBP+DA)-Lips-RVG29.

DA content in the damaged striatum dropped to 21.30% of the control group (Figure 6C). After treatment with (NBP +DA)-Lips-RVG29, the DA level was increased to 76.09%. This increase was greater than that observed in free NBP +DA (32.92%), (NBP+DA)-Lips (44.71%), DA-Lips-RVG29 (55.50%) and NBP-Lips-RVG29 (43.71%). These results confirmed that (NBP+DA)-Lips-RVG29 could effectively reduce 6-OHDA-induced damage to the dopaminergic system.

6-OHDA-induced neurotoxicity promotes the loss of TH-positive (TH^+) neurons, and its loss is correlated with the dopaminergic neurons death.[44] The brain sections of mice were performed for the TH-immunohistochemistry on day 21, and the brown-stained areas consisted of TH^+ neurons (Figure 6D). Compared with the control group, the striatum region of the model mice showed extensive lesions with significantly fewer TH^+ neurons due to 6-OHDA-induced injury to dopaminergic neurons. After treatment with (NBP+DA)-Lips-RVG29, TH^+ neurons in the lesioned striatum were remarkably increased, whereas free NBP+DA, (NBP+DA)-Lips, NBP-Lips-RVG29 and DA-Lips-RVG29 showed weaker therapeutic effects (Figure 6D and E).

As shown in Figure 7A, the levels of oxidative stress-related biomarkers (SOD, G-SH, CAT and T-AOC) in the 6-OHDA group were significantly decreased ($p < 0.001$) compared to those in the control group, indicating a weakened anti-oxidative ability in the lesioned striatum. Consistent with the results of the cell experiments, SOD, G-SH, CAT and T-AOC levels were remarkably restored after treatments, and (NBP+DA)-Lips-RVG29 was the most effective.

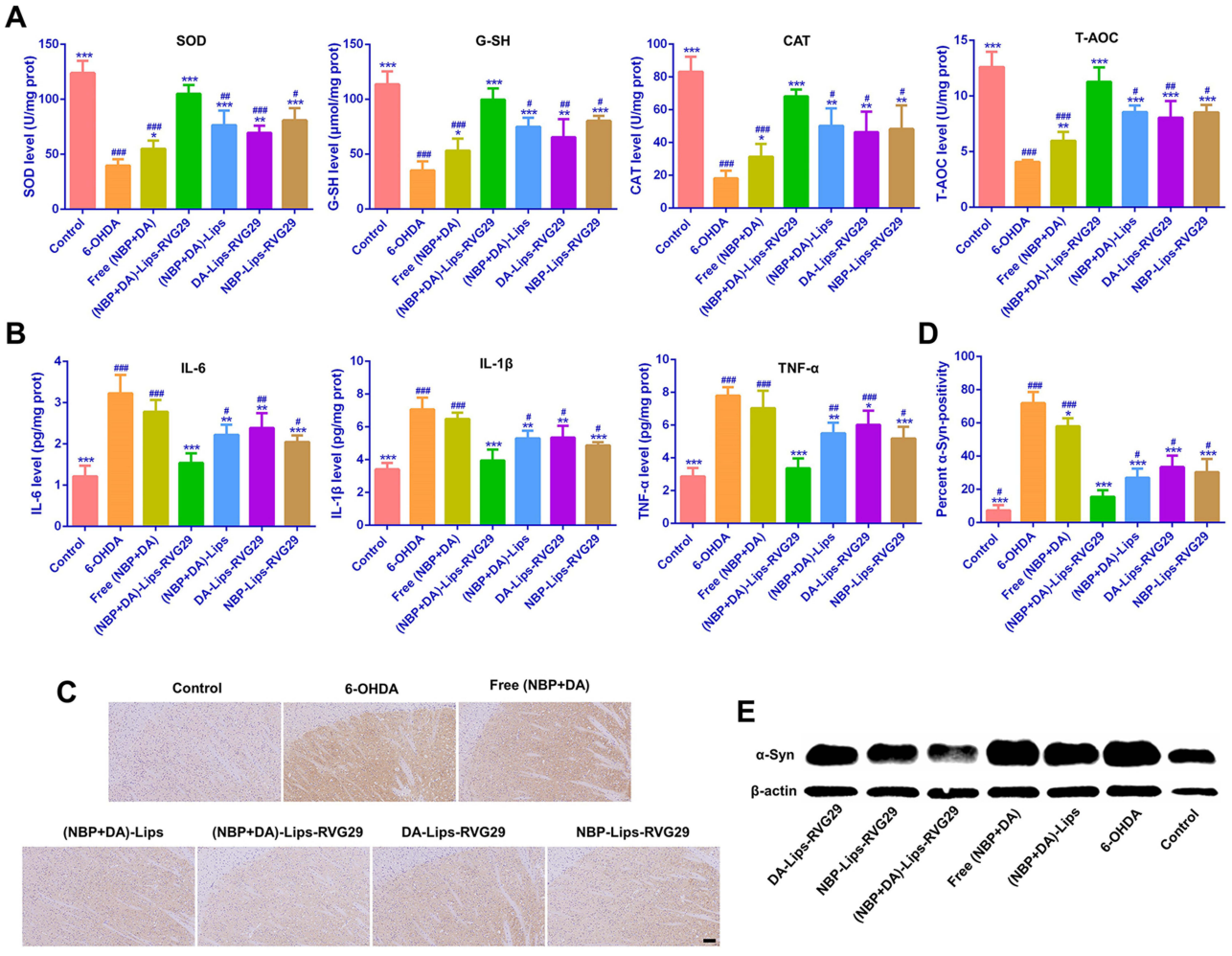

Figure 7 The mechanism underlying therapeutic effect of (NBP+DA)-Lips-RVG29 on PD. (**A**) The levels of SOD, G-SH, CAT and T-AOC in the lesioned striatum of mice in different groups at 21 days after 6-OHDA lesion (mean ± SD, n = 4). (**B**) The level of IL-6, IL-1β and TNF-α in the lesioned striatum of mice in different groups at 21 days after 6-OHDA lesion (mean ± SD, n = 4). (**C**) Immunohistochemistry analysis of α-Syn in the lesioned striatum of mice in different groups at 21 days after 6-OHDA lesion. scale bar: 100 μm. (**D**) The semi-quantitative analysis of α-Syn immunoreactivity (mean ± SD, n = 3). (**E**) The level of α-Syn (14 kDa) expression in the lesioned striatum of mice in different groups at 21 days after 6-OHDA lesion (β-actin: 42 kDa). $^*p < 0.01$, $^{**}p < 0.01$ and $^{***}p < 0.001$ vs 6-OHDA. $^{\#}p < 0.01$, $^{\#\#}p < 0.01$ and $^{\#\#\#}p < 0.001$ vs (NBP+DA)-Lips-RVG29.

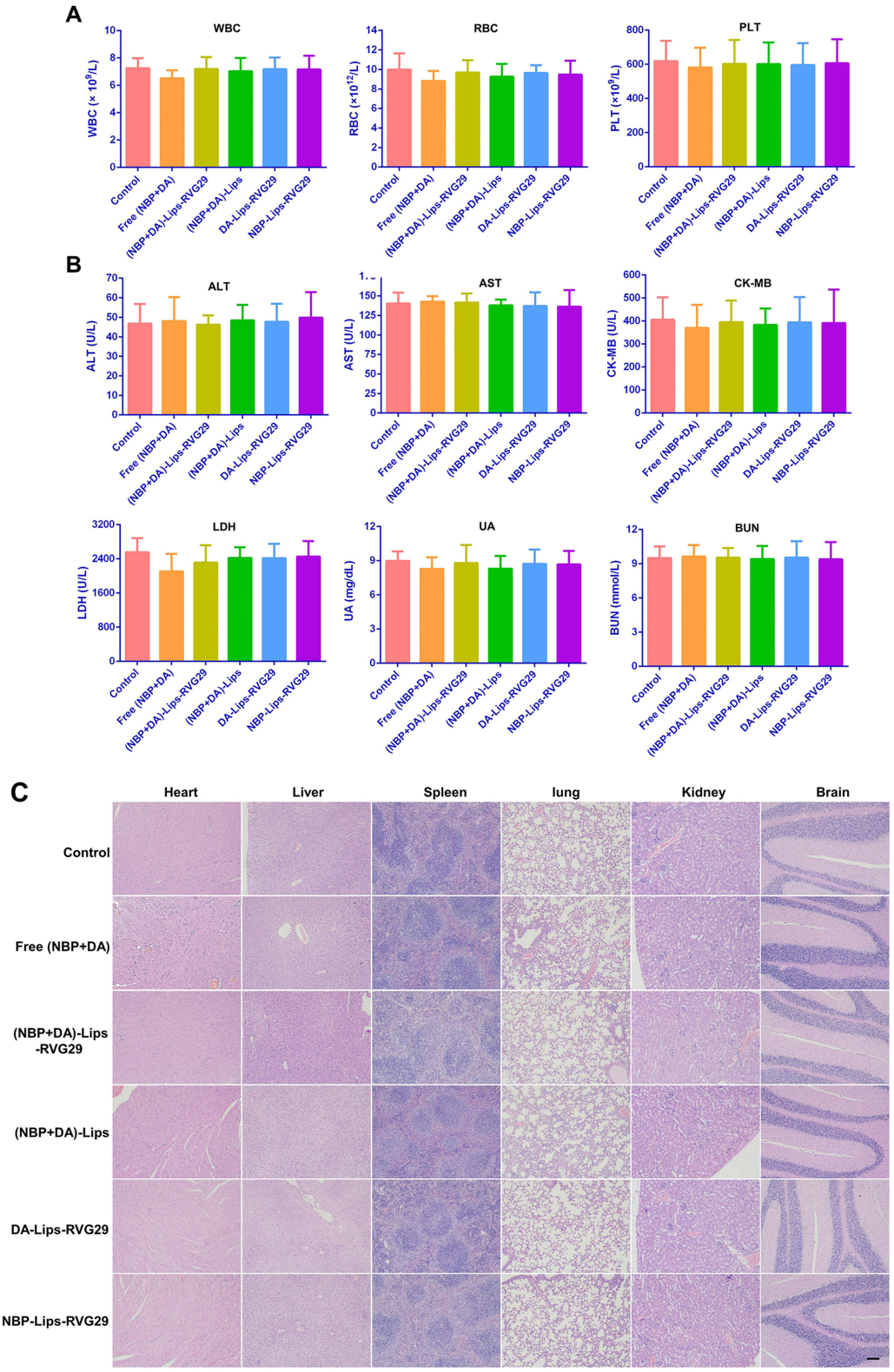

Figure 8 Safety evaluation of (NBP+DA)-Lips-RVG29. (**A**) WBC, RBC and PLT cell counts of mice in different groups. (**B**) ALT, AST, CK-MB, LDH, UA and BUN levels of mice in different groups. (**C**) The tissue morphology (heart, liver, spleen, lung, kidney and brain) of mice in different groups, scale bar: 100 μm.

6-OHDA-induced mice showed higher levels of inflammatory cytokines (IL-6, IL-1β and TNF-α) than those in the control group (Figure 7B). After treatment with different formulations, these parameters decreased to various degrees. (NBP+DA)-Lips-RVG29 showed the greatest decrease among all groups, restoring the levels of IL-6, IL-1β and TNF-α to normal levels. However, the free drugs did not significantly alter inflammatory cytokines levels. It's difficult for free NBP and DA to cross the BBB, which might explain why the therapeutic effectiveness of free drugs in vivo was weaker than that in vitro.

The aggregation of α-Syn is a characteristic of PD, and mutations or overexpression of α-Syn play a crucial role in PD pathogenesis.[45] Oxidative stress and inflammation have been demonstrated to be involved in the overexpression and aggregation of a-Syn.[46,47] In return, pathological a-Syn could induce oxidative stress and neuroinflammation. This vicious circle promotes the development of PD. Immunohistochemical staining of α-Syn showed that the expression of α-Syn in the damaged striatum was significantly increased in the 6-OHDA-treated mice (Figure 7C and D). After treatment, the (NBP+DA)-Lips-RVG29 group exhibited the lowest α-Syn expression level among all groups. In addition, Western blot analysis revealed similar trend (Figures 7E and S3).

Taken together, these findings indicated that NBP and DA could exert their synergistic anti-PD effect through multiple pathways, and (NBP+DA)-Lips-RVG29 is a potential therapeutic candidate for the treatment of PD.

(NBP+DA)-Lips-RVG29 significantly improved the plasma concentration and brain distribution of the drugs. Therefore, it's necessary to evaluate the safety of (NBP+DA)-Lips-RVG29 in vivo. The formulations were injected every other day into mice for 10 times. After 21 days, no significant difference was observed in the blood cell count (WBC, RBC, and PLT) and biochemical parameters (ALT, AST, CK-MB, LDH, UA, and BUN) among the six groups (Figure 8A and B). Moreover, H&E staining of the tissue samples was monitored to further confirm the safety of (NBP+DA)-Lips-RVG29. As shown in Figure 8C, no obvious damage was observed in all tested organs. In general, these results revealed that (NBP+DA)-Lips-RVG29 has good biocompatibility and safety.

Conclusion

A brain-targeting dual-drug liposomes ((NBP+DA)-Lips-RVG29) loaded with NBP and DA at molar ratio 1:1 was successfully prepared, paving the way for the systematic exploration of the combined effects of NBP and DA. This strategy achieved brain neurons-targeting and precise co-localized delivery of NBP and DA by utilizing RVG29-functionalized liposomes as a versatile platform. The clinical translation of nanoparticles faces many challenges. However, both NBP and DA are clinically commonly used drugs, and liposomes are clinically used drug carriers. Our findings may provide a promising approach for the clinical treatment of PD. (NBP+DA)-Lips-RVG29 exhibited satisfactory effect in improving motor behavior, enhancing DA level, attenuating the pathological decrease in TH^+ neurons, reducing oxidative stress and inflammatory response and inhibiting abnormal α-Syn overexpression. Consequently, this combined administration strategy has potential applications in other neurodegenerative diseases therapy.

Acknowledgments

This research was supported by the National Natural Science Foundation of China (No.82104084), CMC Excellent-talent Program of Chengdu Medical College (2024qnGzn12, 2024kjTzn08) and Open Funding of Key Laboratory of Drug-Targeting and Drug Delivery System.

Disclosure

The authors declare no competing interests.

References

1. Hou Y, Dan X, Babbar M, et al. Ageing as a risk factor for neurodegenerative disease. *Nat Rev Neurol*. 2019;15(10):565–581. doi:10.1038/s41582-019-0244-7
2. Li N, Wang L, Zhang J, et al. Whole-exome sequencing in early-onset Parkinson's disease among ethnic Chinese. *Neurobiol aging*. 2020;90:e5–150. doi:10.1016/j.neurobiolaging.2019.12.023
3. Fares MB, Jagannath S, Lashuel HA. Reverse engineering Lewy bodies: how far have we come and how far can we go? *Nat Rev Neurosci*. 2021;22(2):111–131. doi:10.1038/s41583-020-00416-6

4. Elkouzi A, Vedam-Mai V, Eisinger RS, et al. Emerging therapies in Parkinson disease-repurposed drugs and new approaches. *Nat Rev Neurol*. 2019;15(4):204–223. doi:10.1038/s41582-019-0155-7
5. Surendran S, Rajasankar S. Parkinson's disease: oxidative stress and therapeutic approaches. *Neurol Sci*. 2010;31:531–540. doi:10.1007/s10072-010-0245-1
6. Malpartida AB, Williamson M, Narendra DP, et al. Mitochondrial dysfunction and mitophagy in Parkinson's disease: from mechanism to therapy. *Trends Biochem Sci*. 2021;46(4):329–343. doi:10.1016/j.tibs.2020.11.007
7. Tofaris GK. Initiation and progression of α-synuclein pathology in Parkinson's disease. *Cell Mol Life Sci*. 2022;79(4):210. doi:10.1007/s00018-022-04240-2
8. Tansey MG, Wallings RL, Houser MC, et al. Inflammation and immune dysfunction in Parkinson disease. *Nat Rev Immunol*. 2022;22(11):657–673. doi:10.1038/s41577-022-00684-6
9. Huot P, Johnston TH, Koprich JB, et al. The pharmacology of L-DOPA-induced dyskinesia in Parkinson's disease. *Pharmacol Rev*. 2013;65(1):171–222. doi:10.1124/pr.111.005678
10. LeWitt PA, Fahn S. Levodopa therapy for Parkinson disease: a look backward and forward. *Neurology*. 2016;86(14 Supplement 1):S3–S12. doi:10.1212/WNL.0000000000002509
11. Prasad EM, Hung S-Y. Current therapies in clinical trials of Parkinson's disease: a 2021 update. *Pharmaceuticals*. 2021;14(8):717. doi:10.3390/ph14080717
12. Wang S, Ma F, Huang L, et al. Dl-3-n-Butylphthalide (NBP): a promising therapeutic agent for ischemic stroke. *CNS Neurol Disord Drug Targets*. 2018;17(5):338–347. doi:10.2174/1871527317666180612125843
13. Lei H, Zhao C-Y, Liu D-M, et al. l-3-n-Butylphthalide attenuates β-amyloid-induced toxicity in neuroblastoma SH-SY5Y cells through regulating mitochondrion-mediated apoptosis and MAPK signaling. *J Asian Nat Prod Res*. 2014;16(8):854–864. doi:10.1080/10286020.2014.939586
14. Chen Y, Wu T, Li H, et al. Dl-3-n-butylphthalide exerts dopaminergic neuroprotection through inhibition of neuroinflammation. *Front Aging Neurosci*. 2019;11:44. doi:10.3389/fnagi.2019.00044
15. Que R, Zheng J, Chang Z, et al. Dl-3-n-butylphthalide rescues dopaminergic neurons in Parkinson's disease models by inhibiting the NLRP3 inflammasome and ameliorating mitochondrial impairment. *Front Immunol*. 2021;12:794770. doi:10.3389/fimmu.2021.794770
16. Zhao Y, Lee JH, Chen D, et al. DL-3-n-butylphthalide induced neuroprotection, regenerative repair, functional recovery and psychological benefits following traumatic brain injury in mice. *Neurochem Int*. 2017;111:82–92. doi:10.1016/j.neuint.2017.03.017
17. Zhou H, Ye M, Xu W, et al. DL-3-n-butylphthalide therapy for Parkinson's disease: a randomized controlled trial. *Exp Ther Med*. 2019;17(5):3800–3806. doi:10.3892/etm.2019.7397
18. Abbott NJ, Patabendige AA, Dolman DE, et al. Structure and function of the blood-brain barrier. *Neurobiol Dis*. 2010;37(1):13–25. doi:10.1016/j.nbd.2009.07.030
19. Zou Y, Wang Y, Xu S, et al. Brain co-delivery of temozolomide and cisplatin for combinatorial glioblastoma chemotherapy. *Adv Mater*. 2022;34(33):2203958. doi:10.1002/adma.202203958
20. Zhou Y, Peng Z, Seven ES, et al. Crossing the blood-brain barrier with nanoparticles. *J Control Release*. 2018;270:290–303. doi:10.1016/j.jconrel.2017.12.015
21. Baer G, Shaddock J, Quirion R, et al. Rabies susceptibility and acetylcholine receptor. *Lancet*. 1990;335(8690):664–665. doi:10.1016/0140-6736(90)90454-D
22. Gao C, Wang Y, Sun J, et al. Neuronal mitochondria-targeted delivery of curcumin by biomimetic engineered nanosystems in Alzheimer's disease mice. *Acta Biomater*. 2020;108:285–299. doi:10.1016/j.actbio.2020.03.029
23. Wang S, Han Q, Zhou T, et al. A bibenzyl compound 20C protects rats against 6-OHDA-induced damage by regulating adaptive immunity associated molecules. *Int Immunopharmacol*. 2021;91:107269. doi:10.1016/j.intimp.2020.107269
24. Ding T, Wang S, Zhang X, et al. Kidney protection effects of dihydroquercetin on diabetic nephropathy through suppressing ROS and NLRP3 inflammasome. *Phytomedicine*. 2018;41:45–53. doi:10.1016/j.phymed.2018.01.026
25. Li Y, Zhou Y, Qi B, et al. Brain-specific delivery of dopamine mediated by N, N-dimethyl amino group for the treatment of Parkinson's disease. *Mol Pharm*. 2014;11(9):3174–3185. doi:10.1021/mp500352p
26. Qu M, Lin Q, He S, et al. A brain targeting functionalized liposomes of the dopamine derivative N-3,4-bis(pivaloyloxy)-dopamine for treatment of Parkinson's disease. *J Control Release*. 2018;277:173–182. doi:10.1016/j.jconrel.2018.03.019
27. Li W, Yi X, Liu X, et al. Hyaluronic acid ion-pairing nanoparticles for targeted tumor therapy. *J Control Release*. 2016;225:170–182. doi:10.1016/j.jconrel.2016.01.049
28. Huang S, Zhang Y, Wang L, et al. Improved melanoma suppression with target-delivered TRAIL and Paclitaxel by a multifunctional nanocarrier. *J Control Release*. 2020;325:10–24. doi:10.1016/j.jconrel.2020.03.049
29. Zhang Q, Tang J, Fu L, et al. A pH-responsive α-helical cell penetrating peptide-mediated liposomal delivery system. *Biomaterials*. 2013;34(32):7980–7993. doi:10.1016/j.biomaterials.2013.07.014
30. Chen Y, Ip FC, Shi L, et al. Coronin 6 regulates acetylcholine receptor clustering through modulating receptor Anchorage to actin cytoskeleton. *J Neurosci*. 2014;34(7):2413–2421. doi:10.1523/JNEUROSCI.3226-13.2014
31. Rabanel J-M, Piec P-A, Landri S, et al. Transport of PEGylated-PLA nanoparticles across a blood brain barrier model, entry into neuronal cells and in vivo brain bioavailability. *J Control Release*. 2020;328:679–695. doi:10.1016/j.jconrel.2020.09.042
32. Lu W, Tan Y, Hu K, et al. Cationic albumin conjugated pegylated nanoparticle with its transcytosis ability and little toxicity against blood-brain barrier. *Int J Pharm*. 2005;295:247–260. doi:10.1016/j.ijpharm.2005.01.043
33. Qu M, Lin Q, Huang L, et al. Dopamine-loaded blood exosomes targeted to brain for better treatment of Parkinson's disease. *J Control Release*. 2018;287:156–166. doi:10.1016/j.jconrel.2018.08.035
34. Xiang H, Zhang Q, Han Y, et al. Novel brain-targeting 3-n-butylphthalide prodrugs for ischemic stroke treatment. *J Control Release*. 2021;335:498–514. doi:10.1016/j.jconrel.2021.05.045
35. Thiele SL, Warre R, Nash JE. Development of a unilaterally-lesioned 6-OHDA mouse model of Parkinson's disease. *J Vis Exp*. 2012;(60):e3234. doi:10.3791/3234
36. Sun J, Li H, Jin Y, et al. Probiotic Clostridium butyricum ameliorated motor deficits in a mouse model of Parkinson's disease via gut microbiota-GLP-1 pathway. *Brain Behav Immun*. 2021;91:703–715. doi:10.1016/j.bbi.2020.10.014

37. Sharma G, Modgil A, Layek B, et al. Cell penetrating peptide tethered bi-ligand liposomes for delivery to brain in vivo: biodistribution and transfection. *J Control Release*. 2013;167(1):1–10. doi:10.1016/j.jconrel.2013.01.016
38. Tian Y, Lu J, Hao X, et al. FTH1 inhibits ferroptosis through ferritinophagy in the 6-OHDA model of Parkinson's disease. *Neurotherapeutics*. 2020;17:1796–1812. doi:10.1007/s13311-020-00929-z
39. Kim K-A, Kim D, Kim J-H, et al. Autophagy-mediated occludin degradation contributes to blood–brain barrier disruption during ischemia in Bend. 3 brain endothelial cells and rat ischemic stroke models. *Fluids Barriers CNS*. 2020;17(1):1–12. doi:10.1186/s12987-020-00182-8
40. C-MJ H, Zhang L, Aryal S, et al. Erythrocyte membrane-camouflaged polymeric nanoparticles as a biomimetic delivery platform. *Proc Natl Acad Sci U S A*. 2011;108(27):10980–10985. doi:10.1073/pnas.1106634108
41. Subramaniam SR, Chesselet M-F. Mitochondrial dysfunction and oxidative stress in Parkinson's disease. *Prog Neurobiol*. 2013;106:17–32. doi:10.1016/j.pneurobio.2013.04.004
42. Zhang W, Chen H, Ding L, et al. Trojan horse delivery of 4,4′-Dimethoxychalcone for Parkinsonian neuroprotection. *Adv Sci*. 2021;8(9):2004555. doi:10.1002/advs.202004555
43. Kwon K, Jung J, Sahu A, et al. Nanoreactor for cascade reaction between SOD and CAT and its tissue regeneration effect. *J Control Release*. 2022;344:160–172. doi:10.1016/j.jconrel.2022.02.033
44. Chotibut T, Davis RW, Arnold JC, et al. Ceftriaxone increases glutamate uptake and reduces striatal tyrosine hydroxylase loss in 6-OHDA Parkinson's model. *Mol Neurobiol*. 2014;49:1282–1292. doi:10.1007/s12035-013-8598-0
45. Zhang Z, Hou L, Li X, et al. Neuroprotection of inositol hexaphosphate and changes of mitochondrion mediated apoptotic pathway and α-synuclein aggregation in 6-OHDA induced Parkinson′ s disease cell model. *Brain Res*. 2016;1633:87–95. doi:10.1016/j.brainres.2015.12.035
46. Han J, Fan Y, Wu P, et al. Parkinson's disease dementia: synergistic effects of alpha-synuclein, tau, beta-amyloid, and iron. *Front Aging Neurosci*. 2021;13:743754. doi:10.3389/fnagi.2021.743754
47. Long H, Zhang S, Zeng S, et al. Interaction of RAGE with α-synuclein fibrils mediates inflammatory response of microglia. *Cell Rep*. 2022;40 (12):111401. doi:10.1016/j.celrep.2022.111401